CHALMERS
UNIVERSITY OF TECHNOLOGY

TiO2 membrane high-contrast grating reflectors for vertical-cavity light-emitters in the visible wavelength regime

JVST B
Journal of Vacuum Science & Technology B

TiO_2 membrane high-contrast grating reflectors for vertical-cavity light-emitters in the visible wavelength regime

Cite as: J. Vac. Sci. Technol. B **33**, 050603 (2015); https://doi.org/10.1116/1.4929416
Submitted: 28 May 2015 • Accepted: 06 August 2015 • Published Online: 24 August 2015

Ehsan Hashemi, Jörgen Bengtsson, Johan S. Gustavsson, et al.

TiO_2 membrane high-contrast grating reflectors for vertical-cavity light-emitters in the visible wavelength regime

Ehsan Hashemi,[a] Jörgen Bengtsson, Johan S. Gustavsson, and Stefan Carlsson
Photonics Laboratory, Department of Microtechnology and Nanoscience (MC2), Chalmers University of Technology, Gothenburg 41296, Sweden

Georg Rossbach
Laboratory of Advanced Semiconductors for Photonics and Electronics, Institute of Condensed Matter Physics, École Polytechnique Fédérale de Lausanne (EPFL), Lausanne CH-1015, Switzerland

Åsa Haglund
Photonics Laboratory, Department of Microtechnology and Nanoscience (MC2), Chalmers University of Technology, Gothenburg 41296, Sweden

(Received 28 May 2015; accepted 6 August 2015; published 24 August 2015)

In this work, the authors describe a novel route to achieve a high reflectivity, wide bandwidth feedback mirror for GaN-based vertical-cavity light emitters; using air-suspended high contrast gratings in TiO_2, with SiO_2 as a sacrificial layer. The TiO_2 film deposition and the etching processes are developed to yield grating bars without bending, and with near-ideal rectangular cross-sections. Measured optical reflectivity spectra of the fabricated high contrast gratings show very good agreement with simulations, with a high reflectivity of >95% over a 25 nm wavelength span centered around 435 nm for the transverse-magnetic polarization. © *2015 American Vacuum Society*. [http://dx.doi.org/10.1116/1.4929416]

I. INTRODUCTION

A broadband, high reflectivity, low loss mirror is an essential element in vertical-cavity light emitters such as vertical-cavity surface-emitting lasers (VCSELs) and resonant cavity light emitting diodes (RCLEDs). The outcoupling mirror is normally a distributed Bragg reflector (DBR), but recently, high refractive index contrast gratings (HCGs) are being explored as an alternative, since they are believed to offer a number of advantages.[1] Among them are transverse mode and polarization control and a broader reflectivity spectrum than epitaxially grown DBRs. An additional benefit is the possibility to set the resonance wavelength of the VCSEL by the dimensions of the grating.[2] By varying the duty cycle and the period of the grating, while maintaining the same grating layer thickness, the phase of the reflected wave can be altered without affecting the magnitude of the reflection. A change in phase is effectively the same as changing the cavity length, i.e., by varying the lateral parameters of the grating on nearby VCSELs, individual resonance wavelengths can be achieved for devices from the same layer structure. Thus, enabling the fabrication of a multiwavelength VCSEL array where the emission wavelengths of the individual devices are set in one single lithography step.

So far, the HCGs have mainly been explored for VCSELs emitting in the infrared wavelength regime, where lasing under electrical injection has been demonstrated at a wavelength of 850 nm using an AlGaAs/air HCG,[3] at 980 nm with a GaAs/oxide HCG,[4] and at 1550 nm with an InP/air HCG.[5] In all those cases, the top mirror consisted of an HCG in combination with a few DBR $\lambda/4$-thick layer pairs to boost the reflectivity. Recently, there have been some reports where lasing has been achieved under electrical injection in devices where the top DBR has been completely replaced by an HCG, such as a GaAs/air HCG VCSEL emitting at 1060 nm (Ref. 6) and a Si/SiO_2 HCG VCSEL emitting at 1320 nm.[7]

For VCSELs and RCLEDs emitting in the blue–green regime, achieving a high reflectivity broadband DBR is very challenging, due to the lack of lattice-matched materials with large refractive index difference in III-nitride-based materials.[8] An HCG could offer an alternative solution, and possibly with some of the additional HCG benefits mentioned previously. A main challenge in the fabrication of a III-nitride-based HCG is to find a sacrificial layer that can be selectively removed without affecting the HCG layer. There have been a few attempts, such as bandgap-selective photoelectrochemical etching of a sacrificial InGaN superlattice to form an AlGaN HCG membrane,[9] however, with a limited airgap height, and focused-ion-beam etching to create an airgap underneath a GaN-based HCG,[10] an impractical process for device integration on a wafer-scale. In addition, GaN membrane gratings have been fabricated from a GaN-on-Si structure by selective etching of Si,[11–13] but applying this concept to fabricate a bottom mirror in a VCSEL is not straightforward, since growth of high-quality GaN on Si for laser applications is very challenging. Due to the difficulties in realizing a III-nitride based HCG structure with an airgap, a GaN grating reflector without an airgap has been proposed.[14,15] This concept offers a more mechanically rigid structure, but the lower index contrast results in a much smaller fabrication window to achieve a reflectivity above 99% required in VCSELs. Another example with no membrane is an optically pumped GaN-based VCSEL using HCG,[16] in which the grating pattern (1D-photonic crystal) is drilled down to about 0.5 μm through the multiple quantum wells.

[a]Electronic mail: ehsan.hashemi@chalmers.se

In this paper, we present an alternative approach for an HCG for the visible regime, namely a free-standing dielectric HCG in TiO_2. It offers approximately the same high index contrast as that of free-standing GaN HCGs, since the refractive index of TiO_2 is about 2.6 at a wavelength of 450 nm, with a negligible absorption for wavelengths above 400 nm. In addition, the TiO_2 HCG scheme allows for direct integration into many different material systems, since lattice-matching is no longer a prerequisite. The paper is organized as follows: Sec. II describes the design of the HCGs, Sec. III describes the fabrication process, Sec. IV the small-area reflection measurements of the fabricated HCGs, and Sec. V concludes the work.

II. HCG DESIGN

A schematic view of the HCG is shown in Fig. 1(a) including the definitions of the four design parameters: the grating thickness t_g, the airgap height h_a, the grating period Λ, and the duty-cycle. To optimize the design of the gratings, the RicWaA MATLAB package was used,[17] based on the rigorous coupled-wave analysis (RCWA) method.[18] The calculations have been performed for normal incidence, to find the best parameters that yield the highest reflectance, widest bandwidth, and the largest tolerance to physical parameter changes caused by fabrication imperfections. An incident plane-wave was assumed, with the grating infinitely extended in the x and y dimensions, with either transverse-electric (TE) polarization, with electric field along the grating bars, or transverse-magnetic (TM), with electric field perpendicular to them. Moreover, the wavelength was set to 450 nm at which the refractive index of TiO_2 is 2.6, taken from measured ellipsometry data. Figures 1(b) and 1(c) show the reflectance contour plots obtained for both the TE and TM-polarizations at 450 nm wavelength in which the freely suspended TiO_2 gratings with a Si substrate show a reflectance of >99% using the optimized structural parameters. Gratings designed for high reflectivity for TE polarized light have commonly been used by other groups, but we find the gratings designed for high reflectivity for TM polarized light better in our case as they exhibit a larger possible tolerance window, making the grating performance less sensitive to changes in the period and duty-cycle. Please note that Si substrates have been used in the process development instead of GaN substrates to keep the cost low, but the optimized process is fully compatible with GaN substrates.

III. HCG FABRICATION

First, a 400 nm-thick sacrificial layer of SiO_2 is deposited on a Si substrate by plasma-enhanced chemical vapor deposition using an Oxford Plasmalab 100 system followed by the deposition of a 220 nm-thick TiO_2 grating layer by reactive dc sputtering (FHR MS150) with the deposition condition of 1 kW dc power, 4 sccm O_2 flow, 40 sccm Ar flow, 5×10^{-3} mbar pressure, and 300 W RF bias power applied to the substrate table. To pattern the grating, a double layered hard mask is used, consisting of SiO_2 with Ni on top, to improve the side-wall profile at the top of the grating and to facilitate the removal of the Ni-mask layer. The first layer in the hard mask, a 100 nm-thick SiO_2-layer, is deposited by sputtering (FHR MS150). The second layer of the hard mask is then created by patterning electron-beam (e-beam) resist, followed by e-beam evaporation of Ni and lift-off. To obtain sub-10 nm resolution of the Ni-stripes a double layer resist process was adopted based upon the process developed by

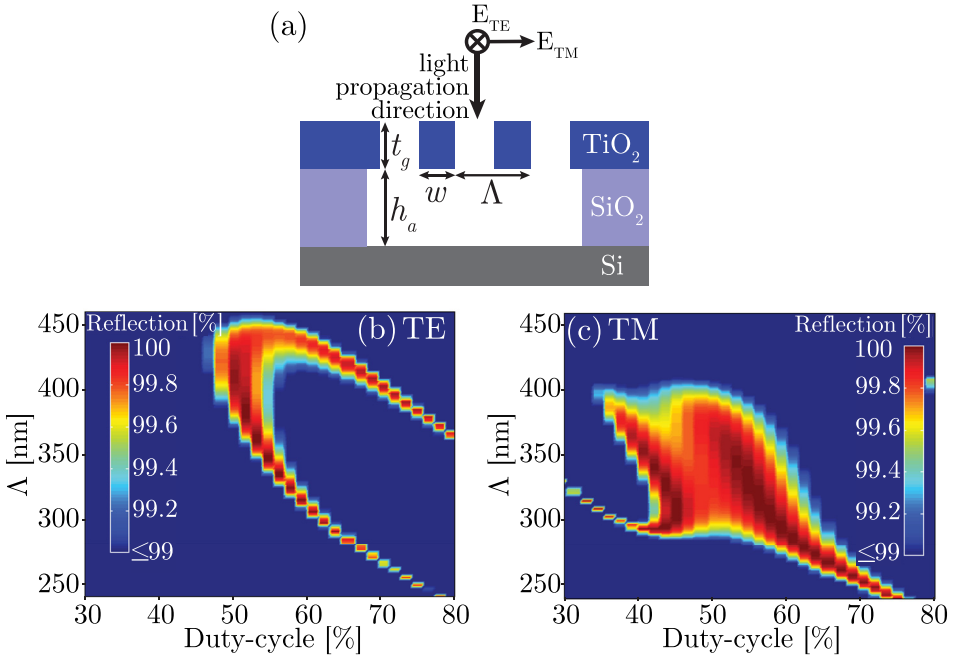

FIG. 1. (Color online) (a) Cross-sectional schematic of a TiO_2/air HCG with a Si substrate. (b) and (c) The reflectance contour plots (>99%) for a wavelength of 450 nm, as a function of grating period Λ and duty-cycle w/Λ, using the optimal layer thickness values for TE polarization: $t_g = 145$ nm, $h_a = 550$ nm, and TM polarization: $t_g = 205$ nm, $h_a = 400$ nm, respectively.

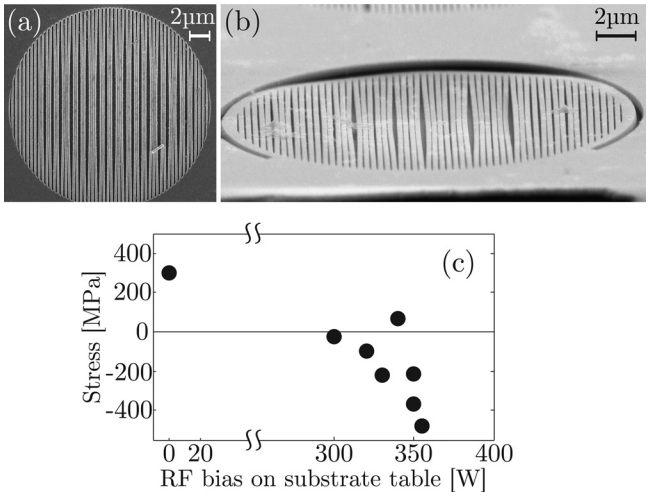

FIG. 2. (a) SEM image of released TiO_2 gratings with very large stress in the film (+300 MPa). (b) SEM image of a grating with stress-relieving trench, but still very large stress in the film (+300 MPa). (c) Stress in the TiO_2 film as a function of different RF power supplied to the substrate.

Rommel *et al.*[19] First, a 70 nm thick poly-methyl-methacrylate (PMMA) layer is spun on and preapplication baked on a hotplate at 160 °C for 5 min to prevent intermixing with the second resist layer. The second layer is a 35 nm thick spin-coated 2% hydrogen silesquioxan (HSQ) layer. The negative HSQ e-beam resist is then pattern exposed in a JEOL JBX-9300FS e-beam lithography system (proximity corrected patterns by dose compensation with a dose in the range of 1.4 mC/cm^2 at 100 kV acceleration voltage). The HSQ is then developed for 60 s in Microposit MF322 and the pattern is transferred into the underlying PMMA layer by O_2/Ar reactive ion etching (RIE). This creates an undercut profile which is suitable for the subsequent lift-off of the 50 nm-thick Ni layer, which is done in 80 °C hot n-ethylpyrrolidone. After the definition of the hard mask, the grating patterns are etched into the TiO_2-layer in an inductively coupled plasma (ICP)/RIE system (Oxford Plasmalab 100). A laser interferometer for *in-situ* monitoring allows monitoring and stopping the etch in the underlying SiO_2 sacrificial layer. The sample is then submerged into a 60 °C-heated Ni-Cr etchant for about 15 min to remove the Ni mask and then immediately dipped into a 1:5 diluted buffered-oxide etch:deionized-water for 4 min to selectively etch away the SiO_2 and release the grating structures. Finally, the liquid is removed from the sample by CO_2 critical point drying to avoid stiction and collapse of the grating bars.

In order to fabricate high-quality free-hanging TiO_2 grating structures, it is essential to both control the stress in the structure and to use optimized etch recipes. The final stress in the TiO_2 film depends on many different factors such as thermal annealing and deposition parameters. Thermal annealing makes the TiO_2 film more tensile, and to produce a low stress film, it is important to minimize the self-heating that occurs during the TiO_2 deposition. The wafers were therefore mounted with thermal tape on a copper chuck to improve the heat dissipation, and several deposition interruptions (5 min deposition/3 min cool-down in open air) were used to minimize the heating. The mounting also led to a more uniform temperature distribution across the wafer and an improved stress uniformity. Besides thermal annealing, deposition parameters also affect the final stress in the film. During the deposition, the RF bias to the substrate table strongly affects the stress in the TiO_2 film, see Fig. 2(c), where a higher RF bias results in a more compressively strained film. A number of samples were deposited with different RF bias to the substrate and gratings were fabricated from them. The stress in the TiO_2 films was estimated by wafer bow measurements. For an RF bias of 0 W, the film had a very strong tensile stress of about +300 MPa, which resulted in severely bent grating bars as seen in Fig. 2(a). Stress-relieving trenches were also incorporated with the grating, since they have the ability to reduce bending of strained bars.[3] For a film with about +300 MPa tensile stress, they reduced the bending to some extent, but instead caused tilting and sagging of the whole structure, see Fig. 2(b). The optimum RF bias was found to be ~300 W, which resulted in a slightly compressive stress in the deposited TiO_2 films between 0 and −100 MPa, and no bending or buckling could be observed in the gratings fabricated from those films (see Fig. 6). These gratings had a bar length of up to 20 μm and a duty cycle between 40% and 60%. If longer grating bars or more narrow bars (lower duty cycles) are to be fabricated, the tolerable stress window will be smaller, since it depends on structural dimensions. It should also be noted that the stress in the final fabricated gratings might differ a bit from that of the film before grating fabrication, and specially designed structures can be incorporated to be able to more locally determine the stress,[20] if this is of interest.

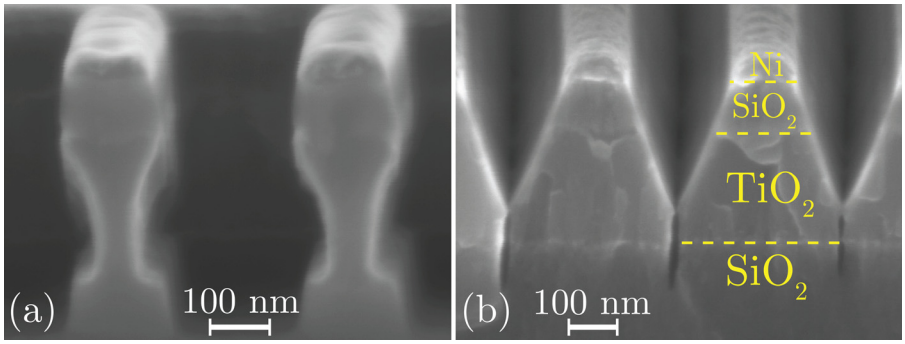

FIG. 3. (Color online) SEM images of the grating in cross-section for an etch recipe with (a) very little polymer formation and (b) higher polymer formation.

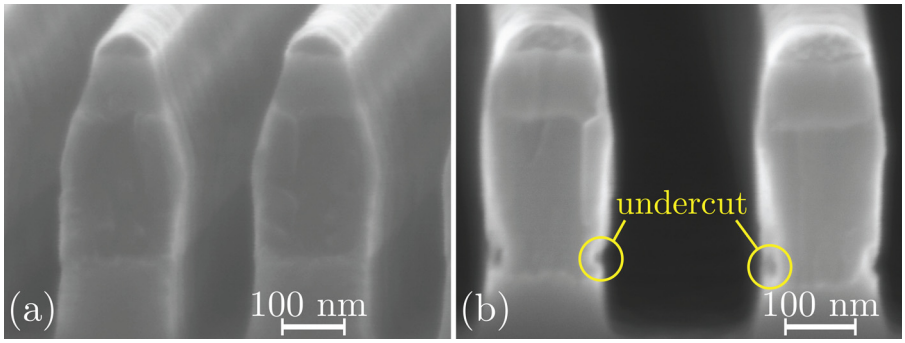

FIG. 4. (Color online) (a) Erosion at the top of the TiO_2 due to high electrode power or very low ICP power. (b) Undercut at the bottom of the TiO_2 due to higher ICP power.

In addition to the stress optimization, it is also important to optimize the dry etching to produce high-quality HCGs. The dry etching was performed in an ICP/RIE Oxford Plasmalab 100 system and as mentioned a combined SiO_2/Ni hard-mask was used to achieve grating bars with more rectangular-shaped cross-section. The etch recipe was optimized with respect to gas chemistry, electrode RF power, ICP power and pressure. Fluorinated gases such as NF_3, CHF_3, CF_4, and SF_6 can be used to etch TiO_2 and SiO_2.[21–24] The carbon-containing gases can also provide sidewall passivation by polymer formation, which is desirable to achieve vertical sidewalls. Comparing CHF_3 with a fluorine-to-carbon ratio (F/C) of 2 to CF_4 which has a higher F/C ratio of 4, the CF_4 yields a more isotropic etch with a very high etch rate [see Fig. 3(a)]. Thus, a CHF_3 plasma is preferred. The polymer formation can be fine-tuned by adding O_2 to decrease the polymer formation or add H_2 to increase it.[25] Figure 3(b) shows an example of the resulting grating cross-section when the polymer formation is very large. The optimized gas chemistry for our gratings was found to be 20 sccm CHF_3 gas with no addition of O_2 or H_2 gases, with a process pressure of 3 mTorr to ensure an anisotropic etch. The electrode and ICP powers were also optimized. An electrode power above 75 W led to a very high erosion of the mask and a very low ICP power yielded a very low etch rate of the oxides, both resulting in a very low selectivity between mask and oxides thus tapered top edges of the gratings [see Fig. 4(a)]. A higher ICP power on the other hand reduced the sidewall passivation at the bottom of the TiO_2 layer, resulting in an undercut profile[26] [see Fig. 4(b)]. The optimized powers were 75 W of electrode power and 180 W ICP power to etch the SiO_2 hard mask and 125 W of ICP power to etch the TiO_2 grating and part of the underlying sacrificial SiO_2 layer. The cross-sectional SEM view of a grating etched with optimized etch parameters is shown in Fig. 5. It should be noted that the optimized etch recipe depends on annealing conditions, and the films used here were not annealed since it resulted in films with higher tensile stress. Figure 6 shows the finally obtained HCG with a period of 350 nm and duty cycle of about 50% after removal of the Ni and the sacrificial layer.

IV. REFLECTANCE MEASUREMENT

The fabricated HCGs were characterized by measuring the reflectivity spectrum in a microreflectance setup [see Fig. 7(a)]. The light from a Xe white light source is tightly focused with a lens, a circular pinhole, and a microscope objective (100× magnification, numerical aperture = 0.5) to a spot size of about 5–10 μm on the grating, which is smaller than the grating diameter of 12 μm. Another aperture with 1.5 mm minimum opening is placed beneath the objective opening, at a distance of 7 mm to the sample, to artificially reduce the acceptance angle of the incident and collected light. The acceptance angle is thus defined by this aperture to $\pm 6^\circ$. Moreover, a polarizer is inserted in the light path to

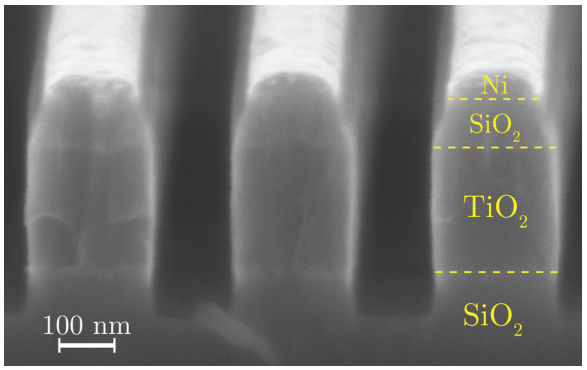

FIG. 5. (Color online) Cross-sectional SEM image of the TiO_2 HCG profile after dry etching using the optimized etch recipe (mixed ICP powers) without annealing.

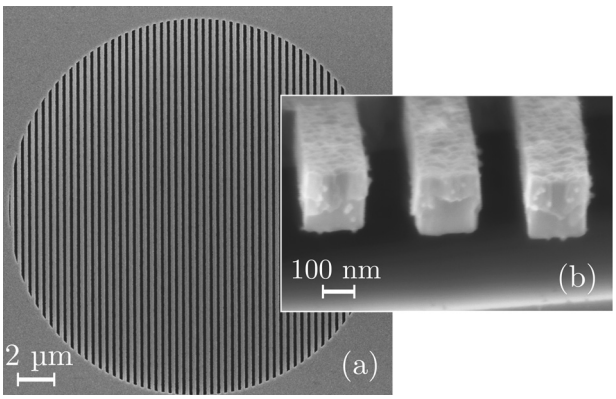

FIG. 6. SEM image of a freestanding TiO_2 HCGs with a period of 350 nm and duty-cycle of about 50% in (a) top view and (b) cross-sectional view.

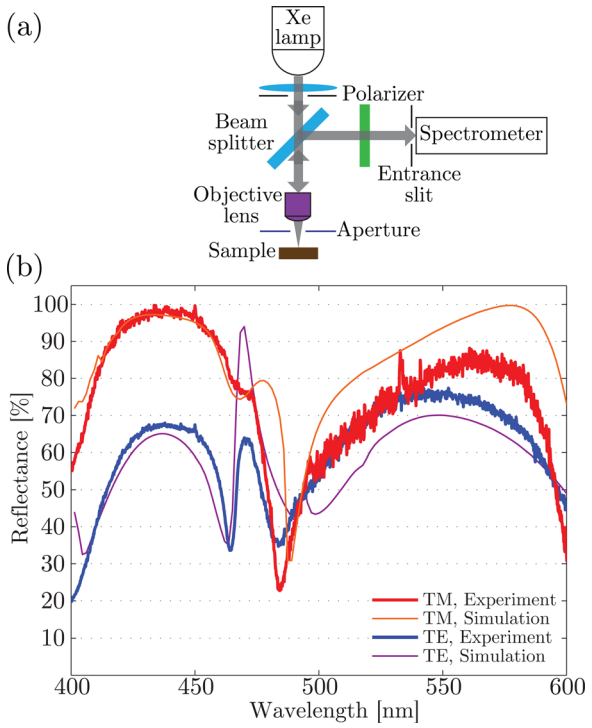

FIG. 7. (Color online) (a) Schematic illustration of the microreflectance setup. (b) Measured and simulated reflectance spectra of the TiO_2 HCG with a period of 370 nm, a duty cycle of about 45%, a grating layer thickness of 210 nm, and an airgap of 340 nm, for both TM and TE polarization.

allow for characterization of polarization dependence of the HCG.

Figure 7(b) shows the measured and simulated reflectance spectra of the TiO_2 HCGs for TM and TE polarized light. A peak reflectance in excess of 95% at 435 nm with a full-width at half-maximum (FWHM) stopband of over 80 nm is achieved for the TM polarization. The peak reflectance for the TE polarization is 30% lower. The reflectivity spectra are also simulated by RCWA method using the actual fabricated grating parameters measured by SEM, the refractive index dispersion of TiO_2 from ellipsometry data, and by considering the reflections from the Si substrate beneath the HCG. The finite acceptance angle is accounted for by averaging the simulated reflectance values for a number of incident angles varying from 0° to 6°. As seen in Fig. 7(b), the agreement between simulated and measured reflectivity spectra is very good, particularly in the 400–460 nm wavelength range.

V. SUMMARY

In summary, we have demonstrated the design and fabrication of air-suspended TiO_2-based HCGs as an enabling technology for high-reflectivity broad spectral bandwidth reflectors for vertical-cavity light emitters in the blue wavelength regime. The measured reflectance spectra of the fabricated gratings agree very well with the RCWA simulations and show a peak reflectivity in excess of 95% at 435 nm, with a FWHM spectral bandwidth of 80 nm for TM polarized light and a much lower reflectivity for TM polarized light. We believe that the proposed scheme can offer an interesting alternative to DBRs in GaN-based VCSELs and RCLEDs.

ACKNOWLEDGMENTS

The authors would like to thank Henrik Frederiksen, Mats Hagberg, and Bengt Nilsson from the MC2 Nanofabrication Laboratory at Chalmers University of Technology for technological support in the processing, and Nicolas Grandjean at EPFL for providing the microreflectance measurement setup. This work was funded by the Swedish Research Council and the Hasselblad Foundation.

[1]C. J. Chang-Hasnain and W. Yang, Adv. Opt. Photonics **4**, 379 (2012).
[2]V. Karagodsky, B. Pesala, C. Chase, W. Hofmann, F. Koyama, and C. J. Chang-Hasnain, Opt. Express **18**, 694 (2010).
[3]M. C. Huang, Y. Zhou, and C. J. Chang-Hasnain, Nat. Photonics **1**, 119 (2007).
[4]P. Gilet, N. Olivier, P. Grosse, K. Gilbert, A. Chelnokov, I. S. Chung, and J. Mørk, Proc. SPIE **7615**, 76150J (2010).
[5]C. Chase, Y. Rao, W. Hofmann, and C. J. Chang-Hasnain, Opt. Express **18**, 15461 (2010).
[6]T. Ansbæk, I. S. Chung, E. S. Semenova, and K. Yvind, IEEE Photonics Technol. Lett. **25**, 365 (2013).
[7]W. Hofmann, C. Chase, M. Muller, Y. Rao, C. Grasse, G. Böhm, M. C. Amann, and C. J. Chang-Hasnain, IEEE Photonics J. **2**, 415 (2010).
[8]D. F. Feezell, Proc. SPIE **9363**, 93631G (2015).
[9]J. Kim, D. U. Kim, J. Lee, H. Jeon, Y. Park, and Y. S. Choi, Appl. Phys. Lett. **95**, 021102 (2009).
[10]T. T. Wu, Y. C. Syu, S. H. Wu, W. T. Chen, T. C. Lu, S. C. Wang, H. P. Chiang, and D. P. Tsai, Opt. Express **20**, 20551 (2012).
[11]N. V. Triviño *et al.*, Appl. Phys. Lett. **100**, 071103 (2012).
[12]Y. Wang, T. Wu, T. Tanae, H. Zhu, and K. Hane, J. Micromech. Microeng. **21**, 105025 (2011).
[13]Y. Wang, Z. Shi, X. Li, S. He, M. Zhang, and H. Zhu, Opt. Express **22**, 667 (2014).
[14]J. Lee, S. Ahn, H. Chang, J. Kim, Y. Park, and H. Jeon, Opt. Express **17**, 22535 (2009).
[15]M. Gebski *et al.*, Proc. SPIE **9372**, 937206 (2015).
[16]T. T. Wu, S. H. Wu, T. C. Lu, and S. C. Wang, Appl. Phys. Lett. **102**, 081111 (2013).
[17]L. Zhang, "RicWaA 1.0.2 MATLAB package," Last accessed September 24, 2013, http://www-personal.umich.edu/~zlei/
[18]M. G. Moharam, T. K. Gaylord, E. B. Grann, and D. A. Pommet, J. Opt. Soc. Am. A **12**, 1068 (1995).
[19]M. Rommel, B. Nilsson, P. Jedrasik, V. Bonanni, A. Dmitriev, and J. Weis, Microelectron. Eng. **110**, 123 (2013).
[20]J. Laconte, D. Flandre, and J. P. Raskin, *Micromachined Thin-Film Sensors for SOI-CMOS Co-Integration* (Springer US, New York, 2006), pp. 47–103.
[21]S. Norasetthekul *et al.*, Appl. Surf. Sci. **185**, 27 (2001).
[22]A. N. Noemaun, F. W. Mont, J. Cho, E. F. Schubert, G. B. Kim, and C. Sone, J. Vac. Sci. Technol. A **29**, 051302 (2011).
[23]K. R. Choi, J. C. Woo, Y. H. Joo, Y. S. Chun, and C. I. Kim, Vacuum **92**, 85 (2013).
[24]A. Matsutani, K. Nishioka, M. Sato, D. Shoji, D. Kobayashi, T. Isobe, A. Nakajima, T. Tatsuma, and S. Matsushita, Jpn. J. Appl. Phys. **53**, 06JF02 (2014).
[25]M. J. Madou, *Manufacturing Techniques for Microfabrication and Nanotechnology*, 3rd ed. (CRC, Boca Raton, FL, 2011), Vol. II, Chap. 3.
[26]N. Rueger, J. Beulens, M. Schaepkens, M. Doemling, J. Mirza, T. Standaert, and G. Oehrlein, J. Vac. Sci. Technol. A **15**, 1881 (1997).